Design Study for the JET Diagnostic
System No. 12.7

BROADBAND CRYSTAL SPECTROMETER FOR THE NON-ACTIVE AND ACTIVE PHASES OF JET

W. Engelhardt, J. Fink, G. Fußmann, H. Krause,
H.-B. Schilling and U. Schumacher

IPP 1/212, IPP III/81 March 1982
Reprint of IPP-JET-Report No. 5

MAX-PLANCK-INSTITUT FÜR PLASMAPHYSIK

8046 GARCHING BEI MÜNCHEN

MAX-PLANCK-INSTITUT FÜR PLASMAPHYSIK

GARCHING BEI MÜNCHEN

Design Study for the JET Diagnostic
System No. 12.7

BROADBAND CRYSTAL SPECTROMETER FOR THE NON-ACTIVE AND ACTIVE PHASES OF JET

W. Engelhardt, J. Fink, G. Fußmann, H. Krause,
H.-B. Schilling and U. Schumacher

IPP 1/212, IPP III/81 March 1982
Reprint of IPP-JET-Report No. 5

Die nachstehende Arbeit wurde im Rahmen des Vertrages zwischen dem Max-Planck-Institut für Plasmaphysik und der Europäischen Atomgemeinschaft über die Zusammenarbeit auf dem Gebiete der Plasmaphysik durchgeführt.

IPP 1/212
IPP III/81

W. Engelhardt
J. Fink
G. Fußmann
H. Krause
H.-B. Schilling
U. Schumacher

Broadband Crystal Spectrometer for the Non-Active and Active Phases of JET

March 1982 (in English)

Abstract

The design study treats the possibilities of quantitatively measuring the Soft X-ray spectrum of JET with a double crystal spectrometer device in parallel mode. This spectrometer type is much suited for broad band soft X-ray spectroscopy, also - due to its folded optical pathway - during D-T operation of JET; the expected detector count rates are far above the background level. Methods to fulfill the important condition of parallel orientation of the two crystals, to shield the device against neutrons and gamma rays, to obtain spectral resolution sufficient for spectral line profile measurements and to upgrade the device for continuous spatial scanning of the JET plasma are presented.

Contents

Part I

1. Task

This study concerns the major properties and design of a diagnostic system for identification and quantitative determination of impurities of the JET plasma in all its operational phases by measurement of the time- and space-resolved X-ray spectrum from the JET discharges.

2. Objectives

Since for JET discharges at temperatures of several keV most of the K-shell resonance lines of metal impurities from wall and limiter materials (Cr, Fe, Ni and Mo) are expected to be emitted, quantitative spectroscopy in the soft X-ray wavelength region (1-100 Å) using crystals is suitable to determine the impurity content, the spatial distribution and the fractional abundances as functions of time.

The objectives of the proposed diagnostic system hence are to obtain values for the concentration of a number of possible impurity atoms expected for the JET discharges as functions of plasma minor radius and time. Therefore a broad-band crystal instrument is desirable, which allows relatively fast scanning of the total spectrum in question. Since the instrument should be applicable in all operational phases of JET, it should be designed also to work for conditions where tritium is used as a fuel component and where high neutron and hard gamma ray fluxes are present.

Crystal spectroscopy offers - due to the relatively large Bragg angles - the possibility to avoid the direct line of sight from the plasma to the detector. Hence, in principle, shielding against

neutron and γ-radiation seems to be possible for the active operation phases of JET. A single crystal spectrometer, which because of shielding requirements cannot easily be installed inside the JET torus hall, asks for relatively large detector displacements if the envisaged soft X-ray wavelength region should be covered. Consequently, massive shielding covering the whole region of detector positions would be necessary.

It is this radiation hardening condition of the broadband crystal spectrometer that asks for consideration of a double crystal spectrometer device. In the following we propose a double crystal spectrometer for broadband soft X-ray spectroscopy, including provisions for line profile measurements, which does not allow spatial scanning. After describing the properties of this device, an extension towards a spatial scan device, one for the active phase (D-T), another for reduced neutron and gamma ray fluxes (D-D-phase), is presented.

3. Principle of the Proposed Double Crystal Broadband Spectrometer

The principle of the proposed double-crystal device for broadband spectroscopy is shown in Fig. 1. The device is thought to be located outside the JET torus hall behind the biological shielding wall. The soft X-rays to be measured pass through a small tube in the wall and - if the Bragg condition is fulfilled - are reflected by the two parallel crystals onto the detector. By this double reflection the outgoing beam is displaced parallel by an amount, which - due to arguments of radiation shielding is of the order on one meter.

The variation of wavelength for the double crystal spectrometer is performed by rotating the crystals into an angular position that corresponds to the Bragg angle and shifting the crystals in parallel directions (see Fig. 1) such, that the beam reflected from the first crystal just hits the center of the second crystal. By this procedure the outgoing beam position is independent of the wavelength such that the detector is at fixed position, which facilitates the vacuum and shielding requirements of the detector.

The important condition for the double crystal spectrometer in

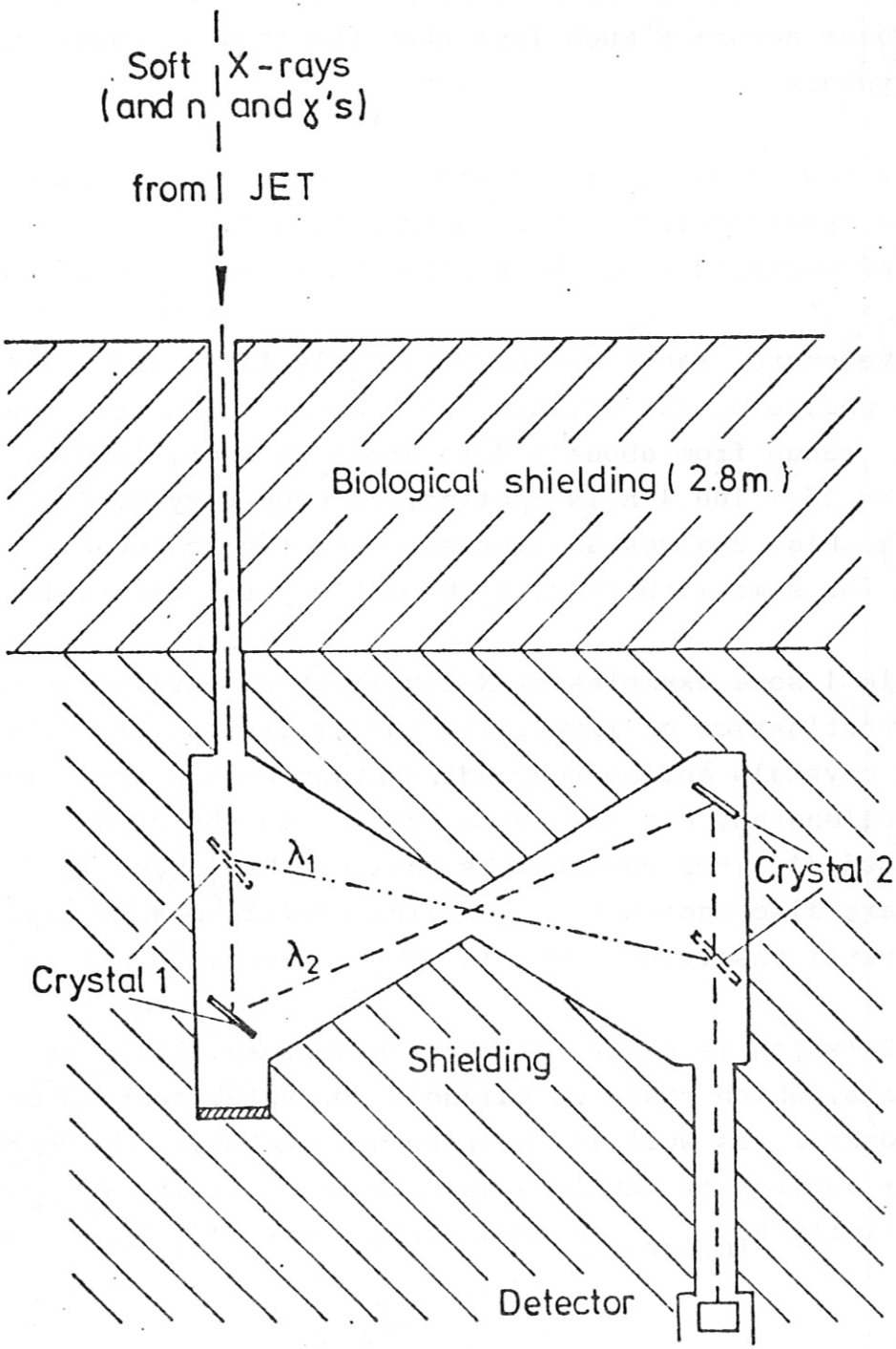

Fig. 1: Principle of the proposed double-crystal broad-band spectrometer

the proposed parallel mode (Fig. 1) is, that both crystals in dispersion direction have to be parallel to each other within an angular accuracy much less than the rocking curve width of the crystals.

The hatched areas in Fig. 1 indicate that the proposed double crystal spectrometer is very much suited for radiation hardening, necessary during the active phase operation of JET.

The wavelength range can be relatively large and - depending on the choice of the crystal - can cover the total wavelenght range from about 1 Å to about 25 Å or, if e.g. Pb-Stearate with its 2d = 100.4 Å is applied, to even very much higher wavelenghts. Fig. 2 gives an impression of the achievable wavelength ranges for some (arbitrarily chosen) crystal materials.

In Table 1 some examples of X-ray lines of particular interest for investigation of impurities in JET plasmas are listed. Suggested crystals and corresponding Bragg angles are related to the wavelengths, and some data concerning the crystal properties are added /1/. For wavelengths smaller than about 10 Å the crystals are also chosen to allow line profile measurements, since the crystal resolving power is then larger or equal to 10^4.

Table 2, which is still somewhat incomplete, lists some crystal materials, which could be suitable for the broadband crystal spectrometer, as well as their lattice spacing 2d, rocking curve width $W_c \equiv d\Theta_1$ for various of wavelengths, peak reflectivity R_{peak}, integral reflectivity $R_{integr.}$ and resolving power /1/, $\lambda/\Delta\lambda = \tan\Theta \cdot d\Theta_1$.

Fig. 2: Achievable wavelength range for a broadband crystal spectrometer

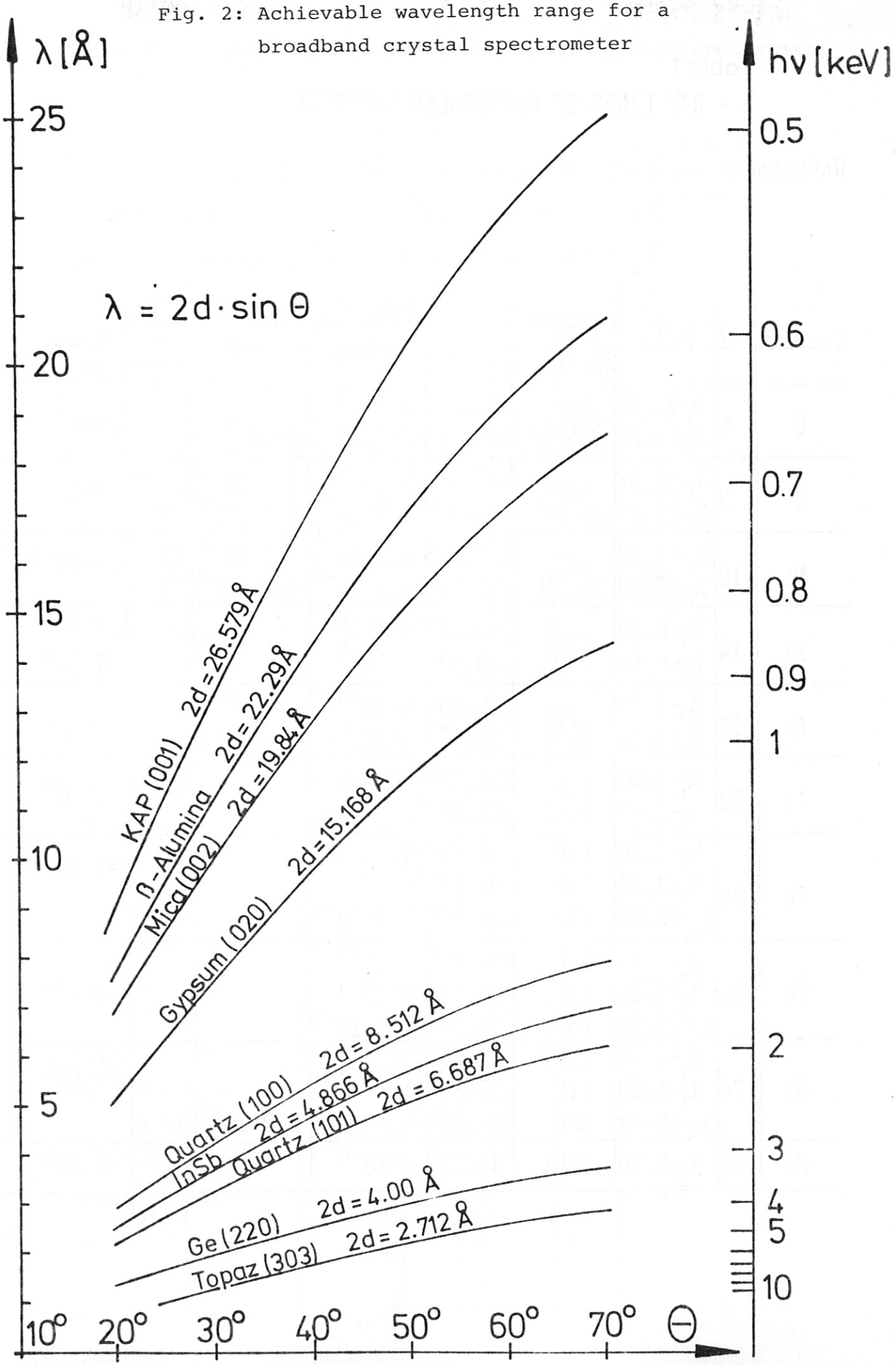

Table 1:

X - RAY LINES OF PARTICULAR INTEREST

WAVELENGTH λ_1 : H - LIKE 1s - 2p - TRANSITIONS

λ_2 : HE- LIKE $1s^2$ - 1s2p $^1P_1$ - TRANSITIONS

λ_3 : NE- LIKE 2p - 3D - TRANSITIONS

ELEMENT	Z	λ(Å)	SUGGEST. CRYSTAL 2D (Å)	θ_0	Integral Reflectivity $R_{integr.}$	Angular width w_C (rad)	Peak Reflect. P(0) [%]	$\lambda/\Delta\lambda$
C	6	λ_1=33.74 λ_2=40.27	PB-STEAR. 100.4	19.65° 23.65°	$2\cdot10^{-4}$ $2\cdot10^{-5}$	$\lesssim1\cdot10^{-2}$		$<10^3$
O	8	λ_1=18.97 λ_2=21.60	KAP 26.58	45.53° 54.36°	$5\cdot10^{-5}$ $5.3\cdot10^{-5}$	$8.7\cdot10^{-4}$ $1.5\cdot10^{-3}$	3.2 2.1	$\approx1\cdot10^3$
NE	10	λ_1=12.13 λ_2=13.44	KAP 26.58	27.16° 30.39°	$6.7\cdot10^{-5}$ $6.3\cdot10^{-5}$	$2.9\cdot10^{-4}$ $4.4\cdot10^{-4}$	15 11.7	$\approx2\cdot10^{+3}$
SI	14	λ_1=6.18 λ_2=6.65	EDDT 8.81	44.58° 49.02°	$5\cdot10^{-4}$ $5\cdot10^{-4}$			$1\cdot10^4$ $1\cdot10^4$
AR	18	λ_1=3.74 λ_2=3.95	EDDT 8.81	25.09° 26.63°	$4\cdot10^{-4}$ $4\cdot10^{-4}$			$1\cdot10^4$
TI	22	λ_1=2.50 λ_2=2.61	LIF 2.85	61.38° 66.41°	$\approx2\cdot10^{-4}$			$4\cdot10^4$
CR	24	λ_1=2.10 λ_2=2.18 λ_3=18.50	LIF LIF KAP	47.51° 50.01° 44.10°	$\approx1\cdot10^{-4}$ $7.3\cdot10^{-4}$			$\approx3\cdot10^4$
FE	26	λ_1=1.79 λ_2=1.85 λ_3=15.01	LIF LIF KAP	38.94° 40.51° 34.39°	$1\cdot10^{-4}$ $1\cdot10^{-4}$ $5.8\cdot10^{-4}$			$\approx2\cdot10^4$
NI	28	λ_1=1.54 λ_2=1.59 λ_3=12.42	LIF LIF KAP	32.73° 33.89° 27.86°	$\approx1\cdot10^{-4}$ $6.7\cdot10^{-5}$	$2.9\cdot10^{-4}$	15.0	$\approx1\cdot10^4$
MO	42	λ_3=5.20	EDDT	36.22°	$5\cdot10^{-4}$			$1\cdot10^4$

Table 2: Crystals suitable for broadband crystal spectroscopy

Crystal	Symbol	2d[Å]	$d\Theta_i$[arcs]	at λ(Å)	R_{Peak}	$R_{integr.}$	Res.pow.
Pb-Stearate		100.4				$3 \cdot 10^{-3}$	
Clinochlore (001)	$Al_2Mg_5Si_3O_{10}(OH)_8$	28.392					1847
KAP (001)	$(OOH)C_6H_4(COOK)$	26.5790				$5 \cdot 10^{-5}$	850
NH_4AP (002)	$(OOH)C_6H_4(COONH_4)$	26.14				$1.5 \cdot 10^{-4}$	1000
β - Alumina	$Na\ Al_{11}\ O_{17}$	22.29					
Mica (002)	$K_2O \cdot Al_2O_3 \cdot 6SiO_2 \cdot 2H_2O$	19.84				$2 \cdot 10^{-5}$	1370
Beryl $(10\bar{1}0)$	$(Be_3Al_2Si_6O_{18})$	15.9549				$6 \cdot 10^{-5}$	1500
Gypsum (020)	$(CaSO_4 \cdot 2H_2O)$	15.168					
ADP (101)	$NH_4H_2PO_4$	10.648				$9 \cdot 10^{-5}$	8200
α - Quartz (100)	SiO_2	8.512					
Quartz $(10\bar{1}0)$	SiO_2	8.35 8.5095	2 4.5 5.5 7 15 23	0.71 1.54 1.85 2.29 3.93 5.0	96.2 85.6 77 72.1 42 18	$6.25 \cdot 10^{-5}$	12300
Indiumantimonide	InSb	7.4866					
Graphite (002)	C	6.708				$1.52 \cdot 10^{-3}$	113
Quartz (101)	SiO_2	6.687					
Quartz $(10\bar{1}1)$	SiO_2	6.592				$1.23 \cdot 10^{-4}$	7700
Potassium Bromide	KBr	6.584					4000
Germanium (111)	Ge	6.533 6.545	7 18 20 25 35 46	0.71 1.54 1.85 2.29 3.95 5.0			3110

Table 2 (continued):

Crystal	Symbol	2d[Å]	$d\Theta_1$[arcs]		R_{Peak} [%]	$R_{integr.}$	Res.pow.
			AT λ(Å)				
Fluorite (111)	CaF_2	6.306					7260
Sylvite (200)	KCl	6.292					6000
Silicon (111)	Si	6.284				$1.2 \cdot 10^{-4}$	7560
Calcite (211)	$CaCO_3$	6.083	14	1.54	45	$4 \cdot 10^{-5}$	12000
				4.66		$1.6 \cdot 10^{-4}$	
Halite (200)	NaCl	5.641					7000
Gypsum (200)	$CaSO_4 \cdot 2H_2O$	5.190					
Quartz ($11\bar{2}0$)	SiO_2	4.913	1.2	0.71			
			1.7	1.54			
			2.0	1.85			
			2.6	2.29			35000
			8.0	3.95		$3 \cdot 10^{-5}$	
Aluminum (111)	Al	4.676					50000
Aluminum (200)	Al	4.057					18000
Lithium Fluoride (200)	LiF	4.027	14	1.54	40	$3 \cdot 10^{-5}$	(500
			CLEAVED				To
			120	1.54	50	$4 \cdot 10^{-4}$	27000)
			ABRADED				
Germanium (200)	Ge	4.000	3	0.71			
			7	1.54			
			8	1.85			
			11	2.29			
				3.46		$2.3 \cdot 10^{-4}$	9000
Silicon (220)	Si	3.840	3	1.54			
				3.32		$8 \cdot 10^{-5}$	
				0.67			17400
Lithium Fluorite (220)	LiF	2.848					33700
Topaz (303)	$(AlF)_2SiO_4$	2.712	14	2.29		$6 \cdot 10^{-5}$	10000
Quartz (310)	SiO_2	2.3604					
Topaz (400)	$(AlF)_2SiO_4$	2.3246	2	1.85		$1 \cdot 10^{-5}$	77000
Quartz (223)	SiO_2	2.028	0.4	0.71			
			0.6	1.54			
Germanium (440)	Ge	2.00	1	0.71			
			3	1.54			
Quartz (502)	SiO_2	1.624					

4. Scientific Specifications of the Proposed Double Crystal Spectrometer

Count rate and time resolution of the double crystal device

For an estimate of brightness of a typical spectral line to be expected for JET we choose the He-like Ni XXVII line at $\lambda = 1.59$ Å with the transition $1s\ ^1S - 2p\ ^1P$. We assume a typical emission length of $l = 100$ cm in JET, an electron density of $3 \times 10^{13}\ cm^{-3}$, an impurity concentration (relative) of $n_{Ni}/n_e = 10^{-3}$ and a temperature of $T = 5$ keV.

For these parameters the photon emission coefficient of this Ni-line is given by

$$\varepsilon[cm^{-3}s^{-1}] = n_e n_{Ni} \cdot f_z \cdot Q,$$

where f_z is the fractional abundance of the ionization state, i.e. Ni^{26+}, and the rate Q is given by Mewe /2/ to be

$$Q[cm^3 s^{-1}] = 1.578 \times 10^{-5} \cdot \left(\frac{\Delta E[eV]}{T_e[eV]}\right)^{1/2} \cdot \frac{f}{\left(E[eV]\right)^{3/2}} \cdot \exp\left[-\left(\frac{\Delta E[eV]}{T_e[eV]}\right)\right] \cdot \bar{g}(y)$$

with the factor

$$\bar{g}(y) = A + Cy + (By - Cy^2 + D)\left(\ln\left(\frac{y+1}{y}\right) - \frac{0.4}{(y+1)^2}\right)$$

and $y = \frac{\Delta E[eV]}{T_e[eV]}$,

where ΔE is the transition energy [in eV], f is the absorption oscillator strength, and A, B, C, and D are adjustable parameters, that in the case of the spectral line in question are given by /2/

$A = 0.04$, $B = 0.06$, $C = -0.04$ and $D = 0.28$.

With $f \simeq 0.79$ and $\Delta E = 7.7987$ keV we obtain

$$y = \frac{\Delta E}{T_e} = 1.5598 \text{ and } \bar{g}(y) = 0.202,$$

so that

$$Q = 9.605 \times 10^{-13}\ cm^3 s^{-1}.$$

Since the fractional abundance f_z of the 26+ ionization state of nickel at an electron temperature of T_e = 5 keV is about /3/

$$f_z \simeq 0.75,$$

we obtain for the volume emission coefficient with an electron density of $n_e = 3 \times 10^{13}\ cm^{-3}$ and a nickel impurity density of $n_{Ni} = 3 \times 10^{10}\ cm^{-3}$ a value of

$$\varepsilon = 6.48 \times 10^{11}\ \text{photons} \cdot cm^{-3} s^{-1}.$$

From this the intensity I results in

$$I = \frac{1}{4\pi} \int_{l_1}^{l_2} \varepsilon\, dl \simeq \frac{\varepsilon}{4\pi} \Delta l$$

with $\Delta l = (l_2 - l_1) = 100$ cm, so that

$$I = 5.2 \times 10^{12}\ \text{photons} \cdot cm^{-2} s^{-1}\ ster^{-1}.$$

The estimate of the count rate of the $(1s\ ^1S - 2p\ ^1P)$ - Ni XXVII spectral line at $\lambda = 1.59$ Å is obtained from the intensity estimate by multiplication with the observable source area S (as determined by the crystal acceptance), the solid angle Ω, the crystal peak reflectivity P(o) and - in the case of the double crystal spectrometer under discussion - with another factor of P(o)/2, which takes the convolution of both crystal profiles into account, and the detector efficiency η. The factor P(o)/2 is derived assuming Lorentzian profiles for the rocking curve which holds for $2d \gtrsim 15$ Å. For smaller crystal spacings the rocking curve approaches a Darwin profile, and the factor is close to P(o).

The source area S is limited by the small crystal acceptance angle ($W_c \approx 10^{-4}$ rad) such that the source width l_s is about equal to the effective crystal width l_c. The source height h_s is not only limited by the diagnostic port height but in the case of high resolution spectroscopy also by the maximum tolerable deviation from the center line Bragg angle Θ_o. This deviation is given by /4/

$$\Delta\theta = \theta_o - \theta = \frac{1}{2}\chi^2 \tan\theta_o \text{ with } \chi \simeq h_s/b,$$

where b is the distance of the crystal from the source. For b = 2000 cm it turns out that $\pm$ 20 cm in vertical (non-dispersive) direction is a limit for which about 10^{-4} spectral resolution can be maintained. Hence $S = h_s \cdot l_s$.

If the crystal height is denoted by h_c, the solid angle is given by

$$\Omega = W_c \cdot h_c/b.$$

Thus the count rate is given by

$$\dot{N} = I \cdot h_s \cdot l_s \cdot \frac{h_c}{b} \cdot W_c \cdot P(o) \cdot \frac{P(o)}{2} \cdot \eta.$$

Since the crystal integral reflectivity R is given by $R = W_c \cdot P(o)$ we have

$$\dot{N} = I \cdot h_s \cdot l_s \cdot \frac{h_c}{b} \cdot R \cdot \frac{P(o)}{2} \cdot \eta.$$

With h_s = 10 cm, l_s = 8 cm, h_c = 4 cm, b = 2000 cm and - choosing Topaz (303) as a suitable crystal - the integral reflectivity /1/ $R = 6 \times 10^{-5}$ and the peak reflectivity of $P(o) \simeq 0.6$ at λ = 1.59 Å we obtain with $\eta \simeq 1$ a count rate of

$$\dot{N} = 1.5 \times 10^7 \text{ s}^{-1}.$$

The detector area has to be at least as large as $h_c \cdot l_c$, i.e. about $5 \times 10 \text{ cm}^2 = 50 \text{ cm}^2$ in order not to reduce the optical beam cross section.

The count rate $\dot{N}$ is much higher than the background count rate of 10^3 s^{-1}, that can be obtained with the shielding arrangement proposed in section 7.2. Thus even very much smaller line intensities can be measured with this device.

There will be enough counts to scan the spectrum by varying the Bragg angle from 30° to 60° in about 1 s. The count number for the Ni XXVII line would be about

$$N \simeq \dot{N} \cdot \Delta\lambda \cdot dt/d\lambda = \dot{N} \cdot \tan\theta \, (\Delta\lambda/\lambda) \, dt/d\theta \simeq 6.5 \times 10^4$$

with $\Delta\lambda/\lambda \simeq 2.7 \times 10^{-3}$ (c.f. section 6).

5. Precision and Adjustment Requirements and Possible Solutions

5.1 Crystal positioning

The crystal spectrometer scheme depends critically on the possibility to control the angular position of the two crystals simultaneously with an accuracy of a few angular seconds during a scan of about 30 degrees. Three different positioning methods have been considered.

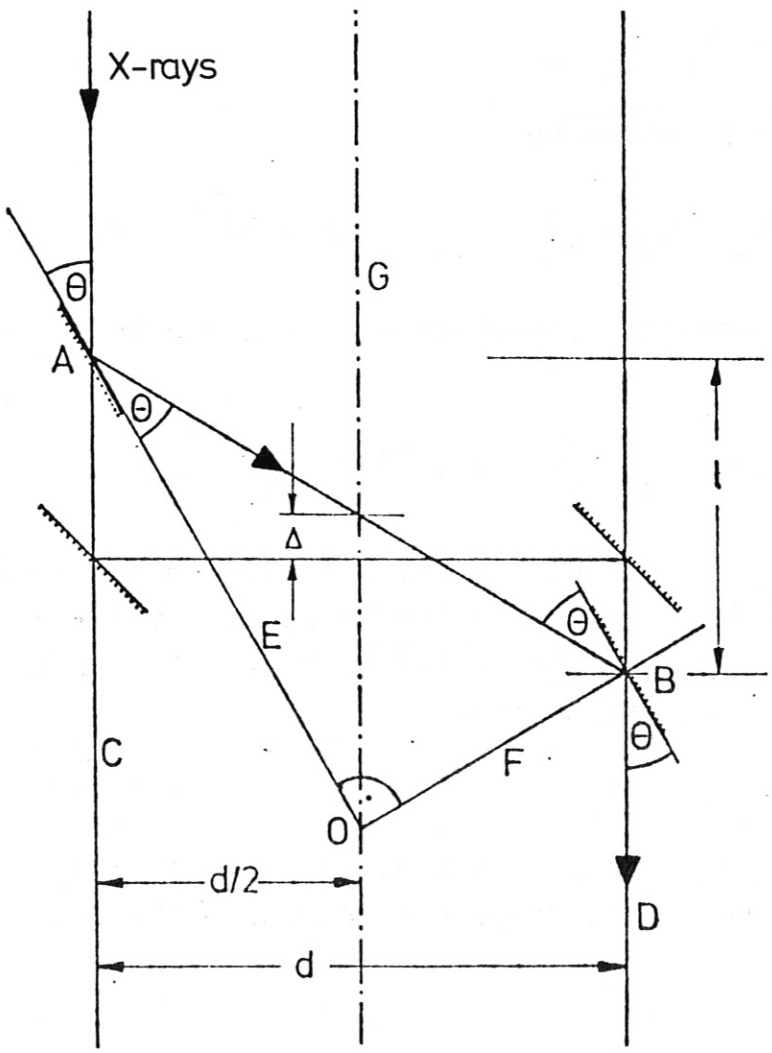

Fig. 3 Mechanical positioning system

A mechanical solution is sketched in Fig. 3. The two crystals A and B glide on the two axes C and D to ensure constant X-ray source and detector positions. In addition the crystals are guided by the two axes E and F which are rigidly connected under 90 degrees. When the connecting device is rotated around the center O, the Bragg angles are changed simultaneously and the positions of the crystals on the C and D axes are set in a way that crystal B is hit by the reflected beam, the beam axis going through the crystal center. If the longitudinal position of the first crystal is fixed (in the spatial scan configuration - as described later) - the rotation center O glides on axis G. This positioning system has been used for a small scale demonstration model. For a full scale device bending forces at the guiding axes E and F owing to inertia and friction would reduce the conformity on the Bragg angles.

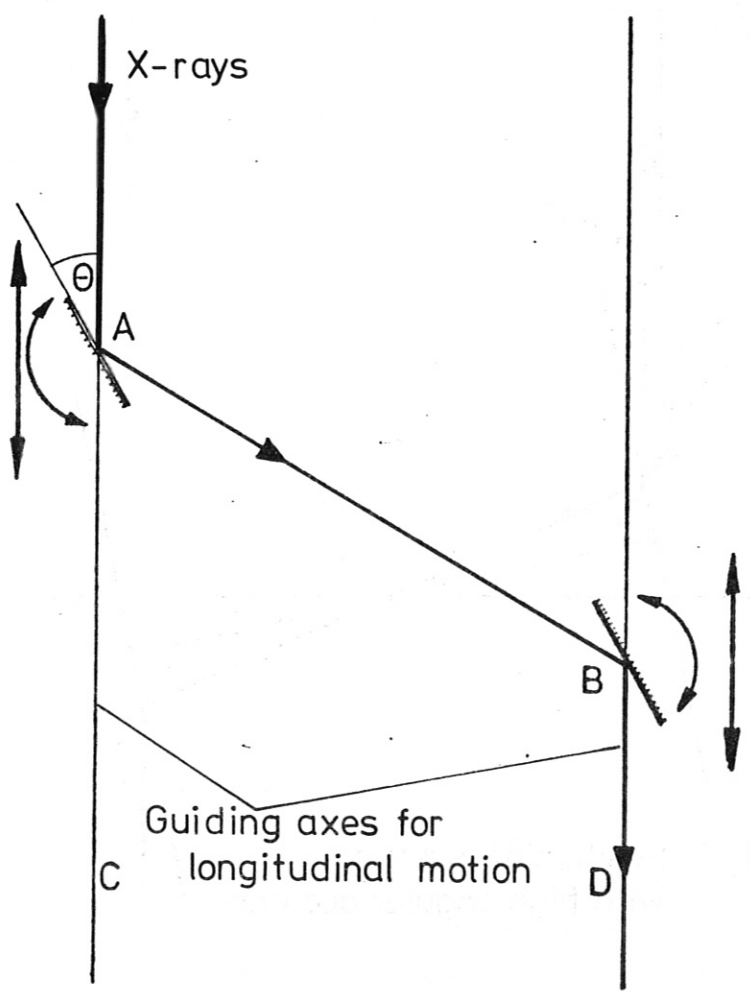

Fig.4 Electronic positioning system

An electronic positioning system which is supposed to give a higher accuracy of the angular positions is shown in Fig. 4. The angular and longitudinal positions of the crystals are independently set by an electronic control system. The accuracy of this system depends on the mechanical accuracy of the longitudinal positioning system, the accuracy of the shaft encorders (see chapter 5.2) and of the control system (see chapter 5.3).

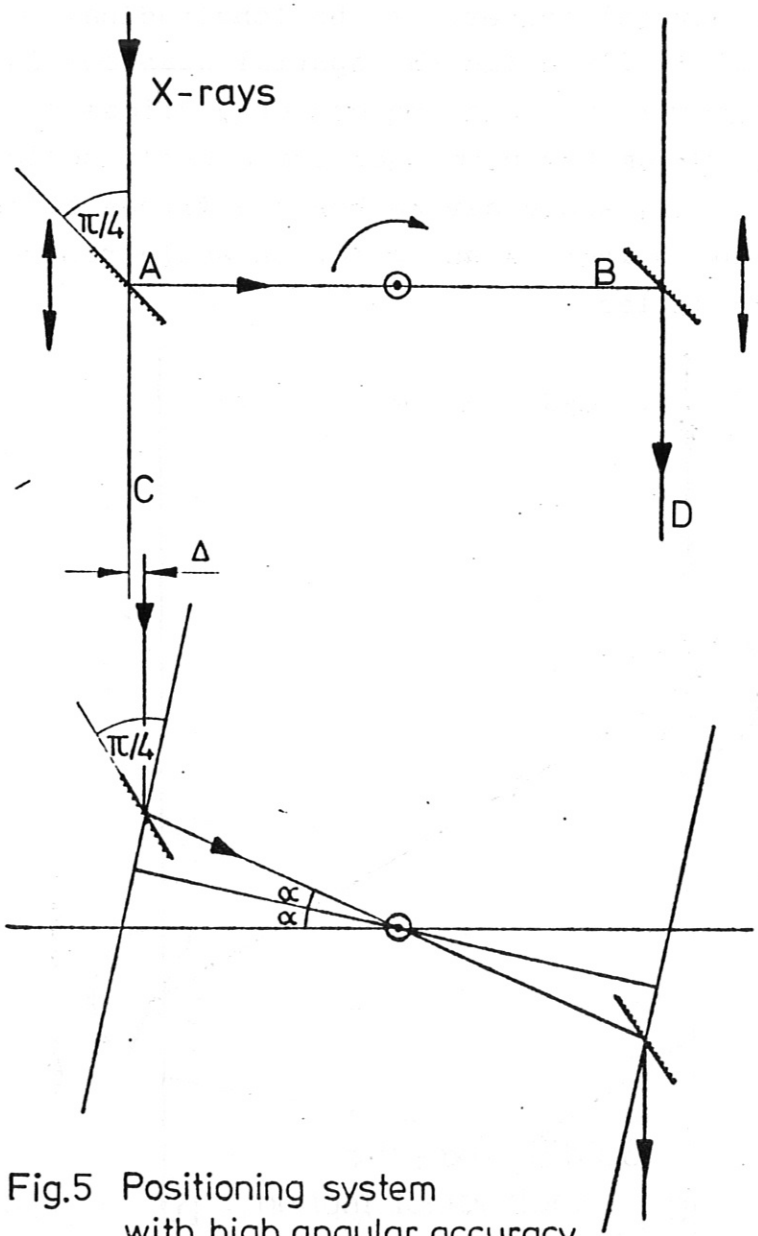

Fig.5 Positioning system with high angular accuracy

A modified electronic solution with intrinsic high accuracy of the Bragg angles is sketched in Fig. 5. The guiding rails are mounted on a ground plate which can be rotated around the center 0. The crystals which are mounted at a fixed angle of 45 degrees with respect to the connecting line A-B glide on the guiding rails C and D. When the Bragg angle is changed from $\pi/4$ to $\pi/4 - \alpha$ by rotating the whole device, by an angle of α (see Fig. 5), the longitudinal position of the crystals on the rails is changed accordingly so that the second crystal center is always hit by the reflected beam axis. The total accuracy of this solution is only limited by mechanical inaccuracies of the linear positioning system.

If the position of the first crystal has to remain constant (in the spatial resolution configuration) - as discussed later - the whole device is rotated around the vertical axis of the first crystal with only one rail for the second crystal. With the modified electronic solution, however, the location of the emerging beam (rotation around the first crystal) or of both the incident and the emerging beam (rotation around the center 0) are no longer constant. An angle different from 90 degrees between the guiding rails and the line A-B may be used to minimize these variations if the Bragg angle is not varied symmetrically to 45 degrees. For large ranges of the scanning angle an additional system for readjusting the detector location has to be employed.

Comparison of the three described devices leads to the result, that the proposed positioning system should be based on the electromechanic solution in its basic version (Fig. 4), which is suitable in particular for larger parallel distances d.

5.2 Positioning elements

Owing to the high demands on angular accuracy the use of step motors (which are only available with low angular resolution) in conjunction with a step-down gear (which would produce considerable backlash) must be excluded. A gearless precision positioning can be achieved by using a combination of DC motors and electro-optical shaft encoders with a computerized control system for position feedback and motion coordination. For the DC motors disc rotor types with constant torque at any angular position and low moment of inertia have been chosen. The static position accuracy

depends only on the type of shaft encoders used.

The output signals of the shaft encoders consists of two sine waves on two separate lines with a phase shift of 90 degrees (Fig. 6) for direction discrimination. For higher resolution these signals can be resolved in amplitude by an external device the output of which again can be resolved in phase. A third output gives a reference position signal for absulute position adjustment and transmission error detection.

For a typical high resolution incremental encorder with 32400 lines per revolution, a standard amplitude resolution by a factor of 5 and an additional phase resolution by a factor of 4 a total resolution of 2 angular seconds can be achieved (Fig. 6). This value has to be added to a possible mechanical error of $\pm$ 2.5 seconds and the mechanical error of the longitudinal positioning system.

If located near the torus (as in the radial scan version) the positioning elements must be radiation resistant. Because commercially available high precision shaft encoders are equipped with semiconductor photoelements, a total dose of 10^5 rad is expected to cause permanent damage of the units.

It is therefore proposed to replace the photoelements by quartz fiberoptics with the optical to electrical transducers located in a safe region. The applicability of fiberoptics athigh radiation levels appears feasible using special fibers. If necessary radiation interference can be cancelled out to a certain extent by using two additional light tubes, one without input signal and one with a constant input signal to separate luminescence and absorption effects. The original signals are regained by subtracting the luminescence signal and multiplying by the reverse gain factor. For the DC motor radiation resistance so far no information is available.

The maximum temperature is 150°C for the motors and 50°C for the shaft encoders in operation. The maximum storage temperature of the shaft encoders is 80°C. In the spatial scan configuration the positioning elements must therefore be cooled during the torus bakeout. The shaft encoders can be operated in vacuum. For the motors no information of vacuum compatibility is available at the moment.

PRINCIPLE:

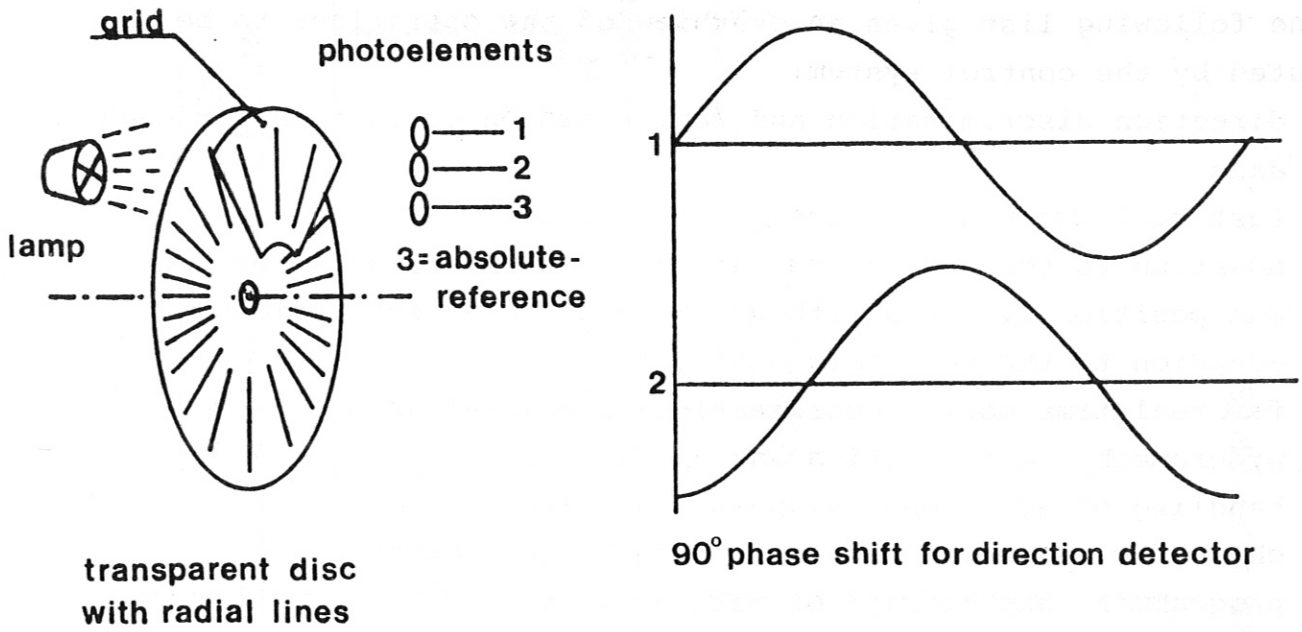

Fig. 6 ELECTRO-OPTICAL INCREMENTAL TRANSDUCERS

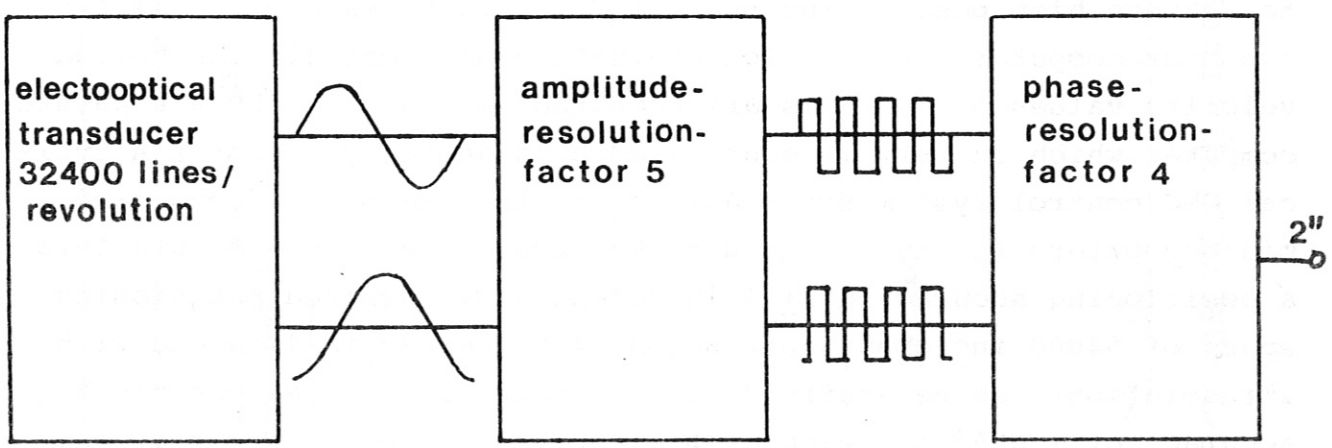

Fig. 7 STANDARD ARRANGEMENT FOR 2" RESOLUTION

5.3 Position control system

The following list gives an overview of the operations to be executed by the control system:

- direction discrimination and real position evaluation for each axis
- fast real time position control for each axis
- adaption to the dynamic characteristics of the axis for maximum positioning speed without overshoot and oscillations
- adaption to the geometric configuration
- fast real time motion coordination of several axes
- programmable acceleration and deceleration
- handling of additional signals (endswitches etc.)
- check for transmission errors and illegal commands
- programming and storage of motion cycles.

These tasks are identical with those to be performed by control systems for industrial robots and other automatic machining devices. The device control section of a commercially available CNC (Computerized Numerical Control) unit for such purposes is sketched in Fig. 8 together with the external positioning elements. In order to achieve high positioning speed and accuracy, each axis has its own microcomputer for position evaluation and control. The nominal velocity values of the axis are computed in real time by a separate computer which in turn is controlled by a geometry computer. A typical CNC control system for 6 axes consists of ~10 interconnected microcomputers for the various tasks. According to the manufacturer a positioning accuracy of $\pm$ 1 increment at the desired positioning speed of 54000 increments per second (30 degrees in 1 second with 2" resolution) can be achieved. This results in a total positioning accuracy of $\pm$ 6.5" for each crystal (2.5" mechanical error of the shaft encoder, 2" of the position control system, 2" quantization error) in addition to the mechanical error of the linear axes. For a spectral line scan for ion temperature measurements of several hundred angular seconds in a time of 0.1 s (or possibly smaller time interval) the same or even a slightly better accuracy can be achieved.

Since the development of a sophisticated position control system requires a lot of know-how, time and money, it is proposed to apply a standard CNC system with some modifications, even when this so-

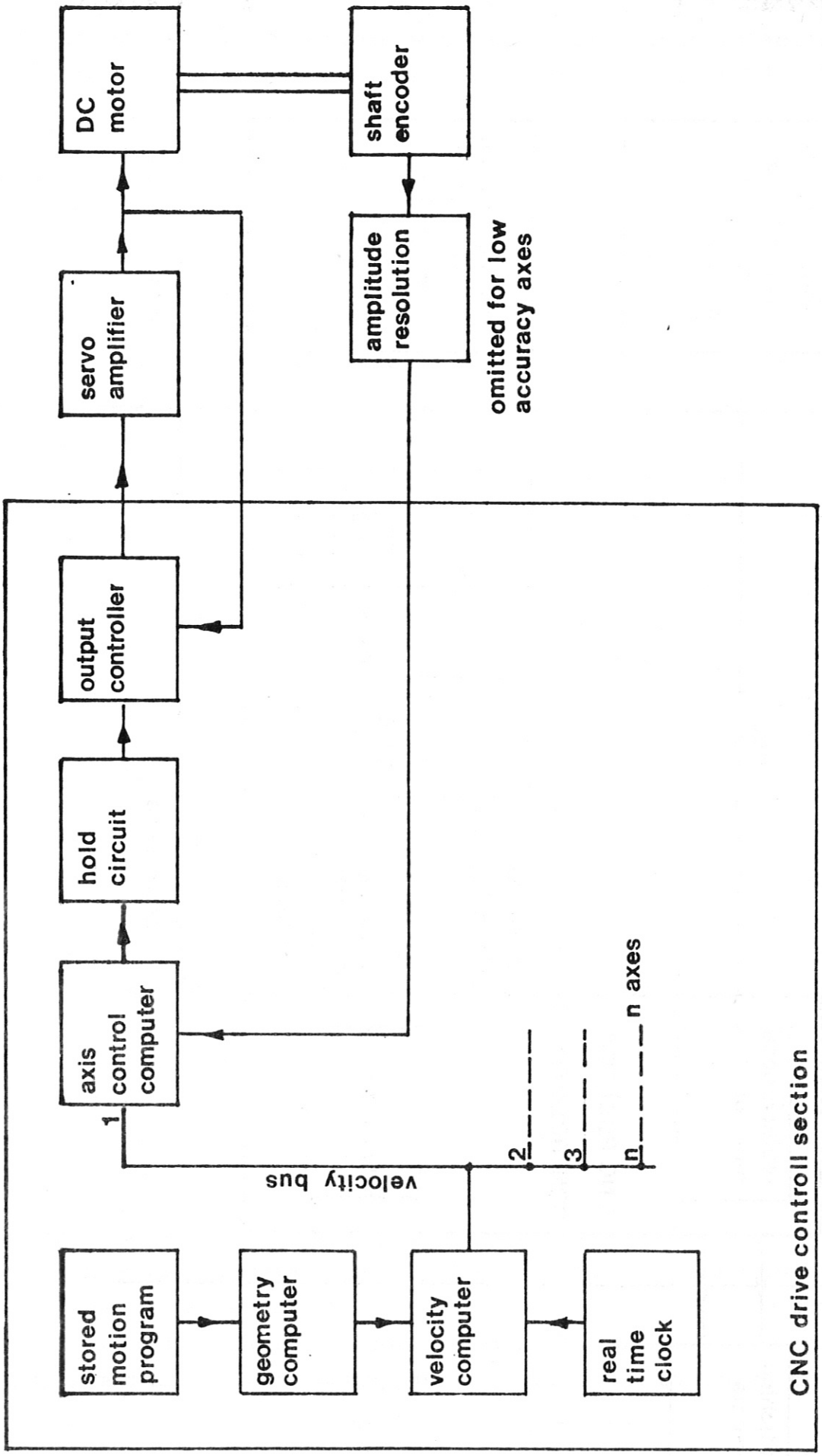

Fig.8 CNC DRIVE CONTROL SECTION WITH EXTERNAL POSITIONING ELEMENTS

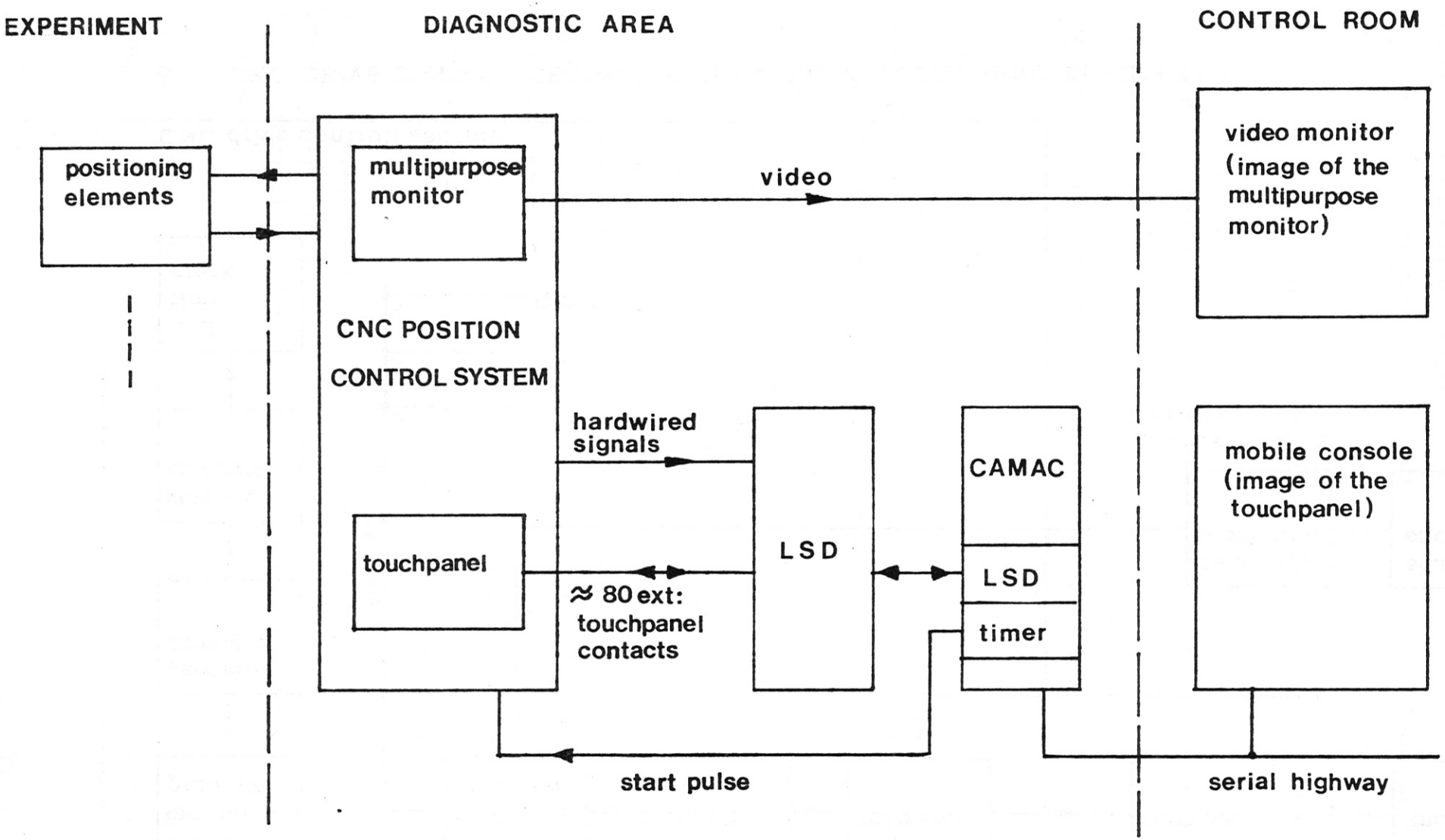

Fig.9 CONNECTION OF THE POSITIONING SYSTEM TO CODAS

lution is not fully compatible with some principles established by JET (no external computer systems, systems without knobs and meters).

5.4 Connection of the positioning system to CODAS

In the standard version the CNC device is controlled locally by a touch-panel and has a multi-purpose monitor for the display of positions, programs, error messages etc. The system can be adapted to CODAS control by adding external contacts for all important touch-panel functions and connecting them to the LSD system (see Fig. 9). An image of the touch-panel has to be implemented on the screen of the mobile console for ease of remote operation. A remote-local switch should be provided. The information of the multi-purpose monitor can, if necessary, be transmitted to an external video monitor in the control room. Some important informations usually displayed on the monitor (e.g. error messages) may, however, be hardwired and connected to the LSD. A transmission of the actual positions of the controlled axes to CODAS is not necessary. Owing to the self-testing facilities the position control system can be relied on to perform the programmed motion, unless an error message is issued.

5.5 Data acquisition of the detector signal

The signal processing of the detector signal is shown in Fig. 10. The signal is amplified by a preamplifier close to the detector and converted to a standard shape by a shaping amplifier. A pulse height discriminator is used to reject counting pulses of undesired events. The selected counting pulses are counted by a latching scaler. With each latching pulse the scaler contents is transferred to a memory. The latching pulses are generated by a time sequence generator, which can be set by software. For a latching period of 1 ms a time span of 16 seconds can be recorded with one memory.

The detector would be a multiwire proportional counter (MWPC) of the desired large area (about 50 cm^2) in order to provide large maximum count rates in the order of $2 \times 10^7 s^{-1}$, made of wires with about 0.1 cm distance. This large area detector can be covered with a thin (0.4 µm) Formvar window. The pulses from each wire are discriminated and added without delay, such that delay line techniques are not necessary.

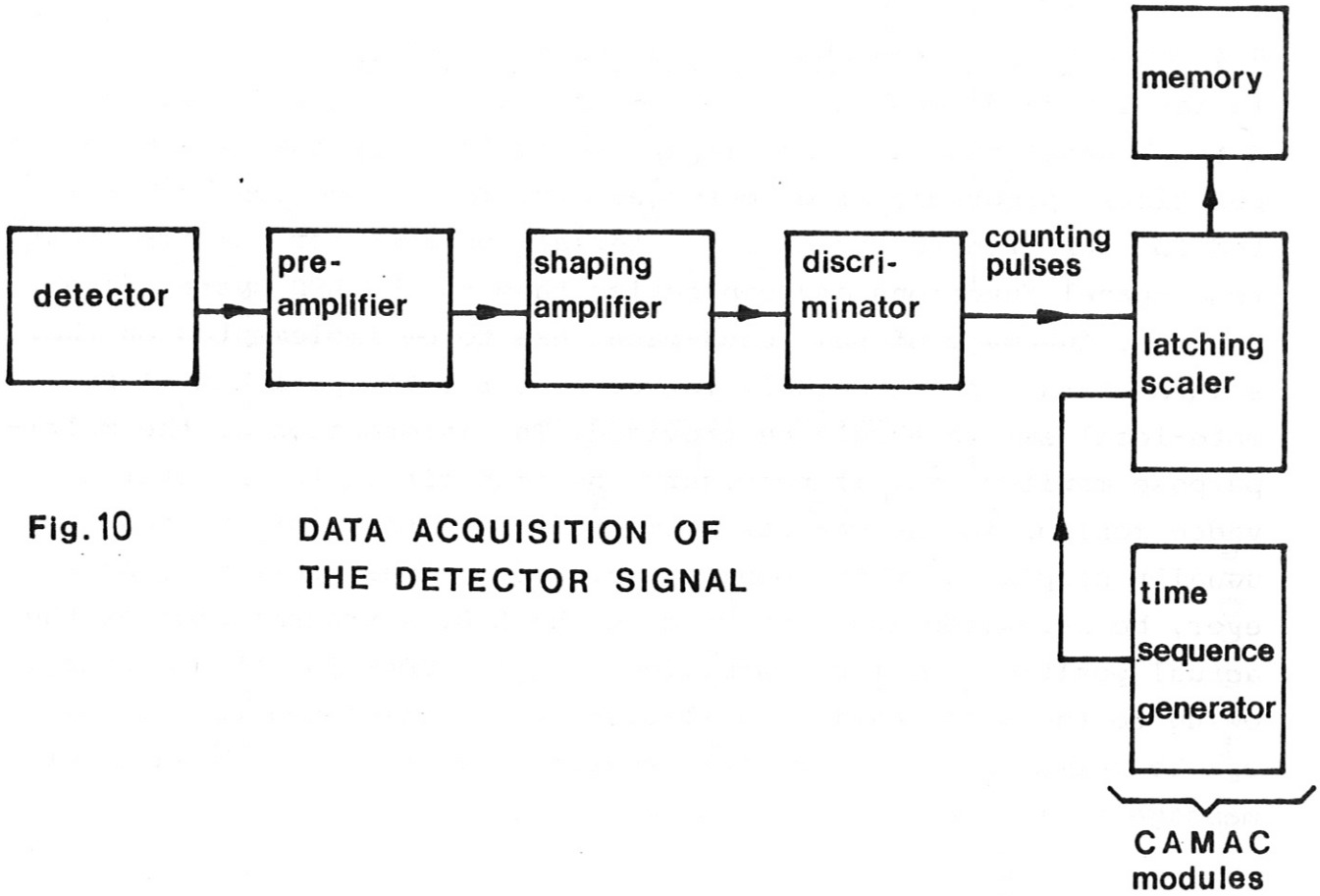

Fig.10 DATA ACQUISITION OF THE DETECTOR SIGNAL

6. High spectral resolution version

The double crystal spectrometer device in the parallel mode (as sketched in Fig. 1) has only moderate spectral resolution. If Θ is the Bragg angle, l the width of the crystals, d the distance of the emerging from the incoming beam and a the source distance from the first crystal, the relative wavelength interval passing the device is given in first order (see Fig. 11)

$$\frac{\Delta\lambda}{\lambda} \simeq \frac{l \cdot \cos\Theta}{\left[\left(a + \frac{d}{\sin 2\Theta}\right)^2 + \left(\frac{l}{2}\sin\Theta\right)^2\right]^{1/2}}$$

which for $l \ll d \ll a$ in the Bragg angle region of

$$\frac{\pi}{6} \lesssim \Theta \lesssim \frac{\pi}{3}$$

is approximated by

$$\frac{\Delta\lambda}{\lambda} \simeq \frac{l \cdot \cos\Theta}{a + \frac{d}{\sin 2\Theta}} \quad ,$$

so that for the parameters chosen in chapter 4 (a = 2000 cm, d = 100 cm, l = 8 cm, $\Theta = \frac{\pi}{4}$) we arrive at

$$\frac{\Delta\lambda}{\lambda} \simeq 2.7 \times 10^{-3},$$

which is not sufficient for spectral line profile measurements.

A double crystal spectrometer in the non-parallel mode inherently has high spectral resolution, if crystals of relatively small rocking curve widths are chosen. Its application, however, needs provisions for moving the detector as well as both crystals, and hence difficult mechanical, vacuum and shielding implications are foreseen, if the wavelength should be varied over a relatively wide region.

In order to perform spectral line profile measurements for temperature determination with a double crystal spectrometer in the proposed parallel mode, a high transmission collimator is necessary. One possible type is the grid-collimator /6,7,8/. This collimator

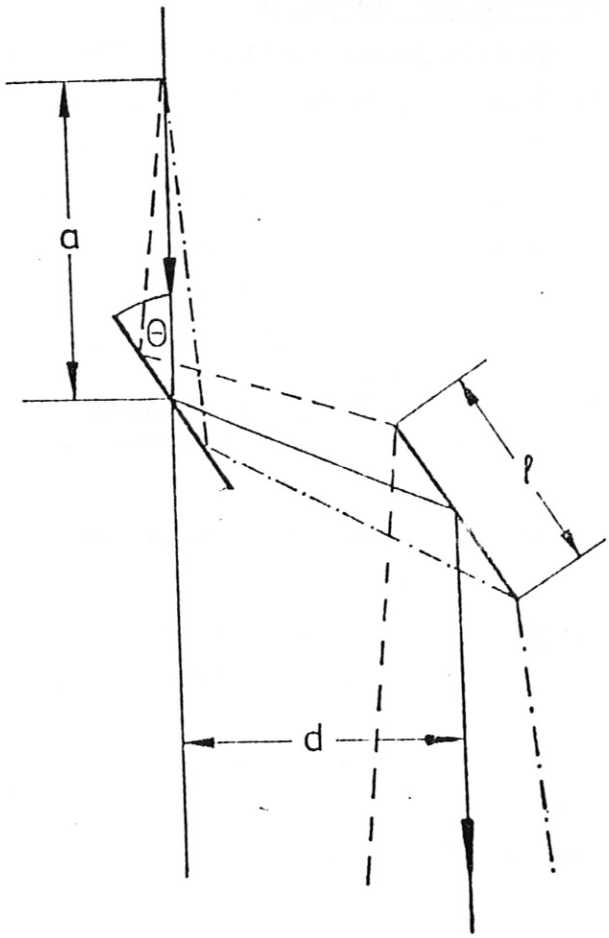

$$\frac{\Delta\lambda}{\lambda} \simeq \frac{\ell \cos\theta}{\left[\left(a + \frac{d}{\sin 2\theta}\right)^2 + \left(\frac{\ell}{2}\sin\theta\right)^2\right]^{1/2}}$$

Fig. 11 Passing wavelength interval for double crystal device in parallel mode

consists of a few planes formed by equidistant parallel grids, the principle being demonstrated by the sketch in Fig. 12. It is obvious that the relatively large angle accepted by the double crystal device in parallel mode (Fig. 11) can be reduced appreciably in order to meet the desired spectral resolution. The grids can be formed whether by wires on a frame or as fine

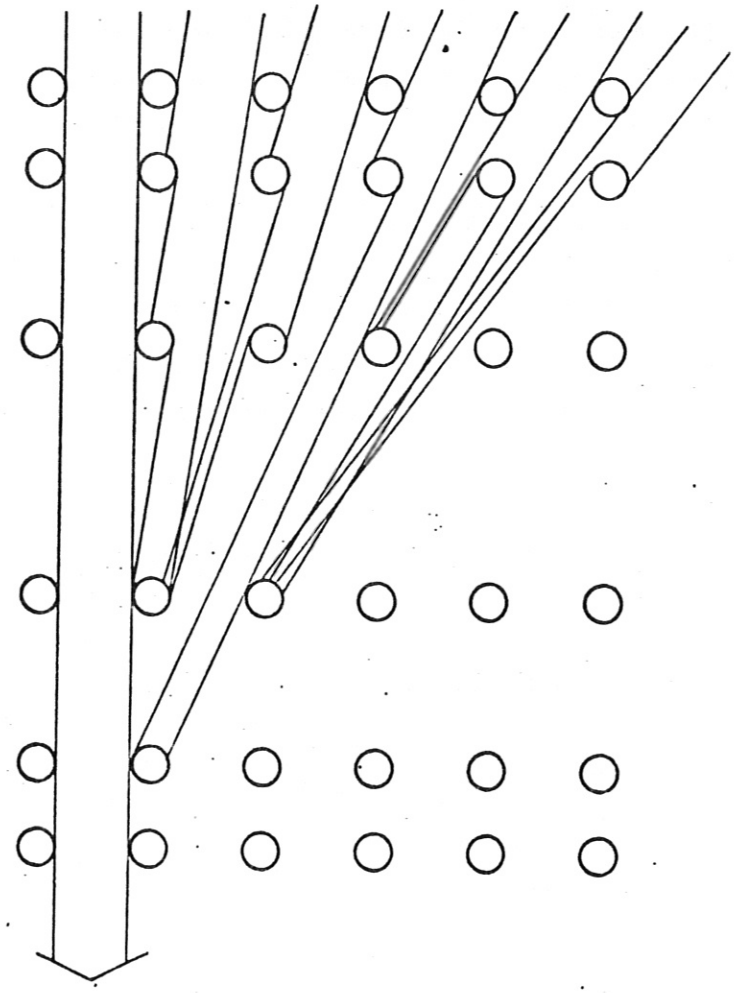

Fig. 12 Schematic of a grid-collimator

mesh electroformed grids, fabricated by industry. The collimator transmission increases with the ratio of the wire diameter versus the free space between the wires.

The location of the collimator can be somewhere between the plasma and the first crystal or between the second crystal and the detector. Because of accessibility reasons and easier plugging it in or taking it out in between different shots, we would prefer a location in front of the detector as indicated in Fig. 13 a.

In the following we treat the conditions for the application of such a gridded collimator to perform line profile measurements for ion temperature determination. We assume the same parameters as already chosen for the estimates in section 4.

For the estimate of the tolerable background noise level we assume an apparatus profile which is about 1/3 of the full line half width of the Doppler profile at $T_i=T_e=5$ keV and furthermore ask for a measurement of the profile in the wings down to an intensity of 20 % of the maximum (central) intensity. Since the full half-width $\Delta\lambda_D$ of the Doppler broadening is given by

$$\Delta\lambda_D = \frac{2(2\ln 2)}{c}^{1/2}\left(\frac{kT_i}{M_i}\right)^{1/2} = 2.435 \times 10^{-3}\left(\frac{kT_i[\mathrm{keV}]}{A}\right)^{1/2}$$

the apparatus profile width should be

$$\frac{\Delta\lambda}{\lambda} = \frac{1}{3}\ \frac{\Delta\lambda_D}{\lambda} = 2.37 \times 10^{-4}$$

for kT_i = 5 keV and Ni-lines (A = 58.7)

With this apparatus profile - assuming the collimator transmissivity to be about T_c = 0.5 - one obtains a count rate of about $2.5 \times 10^6\ s^{-1}$ in the line center and about $5 \times 10^5\ s^{-1}$ in the wings, which is down to 1/5 of the maximum (central) intensity. Hence about $5 \times 10^5\ s^{-1}$ would be a tolerable background count rate. For a detector area of 5 x 10 cm^2 = 50 cm^2 the tolerable gamma flux (at about 2 % detectivity for 1 to 2 MeV gammas) would be about $5 \times 10^5\ cm^{-2}s^{-1}$. In order to be able to measure under less favourable conditions, somewhat arbitrarily a background count rate of only $10^3 s^{-1}$ is aimed at for the outlay of the shielding arrangement (c.f. section 7.1).

An estimate of the achievable time resolution for a line profile measurement is made under the assumption that 1000 counts are necessary for this measurement /7/. Therefore we represent the count rate of the Doppler line profile by

$$\dot{n}(x) = \dot{N} \cdot T_c \cdot \pi^{-1/2} \cdot \exp(-x^2)$$

with $x = \Delta\lambda / \Delta\lambda_D$ the relative wavelength difference and $\dot{N} = \int_{-\infty}^{+\infty} \dot{n}(x)\, dx$ the total line count rate, T_c the collimator transmissivity.

If the wavelength is changed between the values x_1 and x_2 with constant speed $\frac{dx}{dt}$ we obtain with $\frac{dn}{dx} = \dot{n}\,\frac{dt}{dx}$ the total count number N of the line to be

$$N = \int_{x_1}^{x_2} \frac{dn}{dx}\, dx = \frac{dt}{dx} \int_{x_1}^{x_2} \dot{n}(x)\, dx = \frac{T}{x_2 - x_1} \int_{x_1}^{x_2} \dot{n}(x)\, dx,$$

where T is the time interval for the scan over the total line profile from x_1 to x_2, and T is connected with the mean count rate

$$\bar{\dot{n}} = \frac{1}{x_2 - x_1} \int_{x_1}^{x_2} \dot{n}(x)\, dx$$

by $T = \frac{N}{\bar{\dot{n}}}$.

The mean count rate $\bar{\dot{n}}$ is related to the total count rate $\dot{N}$ of the line by

$$\bar{\dot{n}} = \dot{N} \cdot T_c \frac{2}{\pi^{1/2}} \cdot \frac{1}{2x} \int_0^x \exp(-x'^2)\, dx' = \frac{\dot{N}}{2} \cdot \frac{\mathrm{erf}(x)}{x} \cdot T_c .$$

If we take a wide wavelength range for the scan, i.e. $x \simeq 5$, we obtain

$$\bar{\dot{n}} = \frac{\dot{N}}{2} \cdot T_c \cdot \frac{\mathrm{erf}(5)}{5} \simeq 0.1 \cdot \dot{N} \cdot T_c$$

and with $N = 10^3$ and $\dot{N} \cdot T_c = 7.4 \times 10^6\ s^{-1}$ the achievable time resolution is about

$$T \simeq 1.3\ ms,$$

which is very much less than the expected energy confinement time.

7. Neutron and Gamma Ray Shielding

7.1 Shielding Requirements

During deuterium-tritium discharges the JET plasma is expected to emit up to 6×10^{19} neutrons (of 14 MeV) per second at a corresponding α-particle heating power of 34 MW /9/. This neutron source strength will result in fluxes /10/ of about 2×10^{12} n/(cm^2 · s) and about 7×10^{11} γ/(cm^2 · s) near the inside of the walls of the torus hall. Due to the high neutron albedo of the walls of some 60 % about half of this neutron flux will be isotropic due to single and multiple backscattering from the walls, the other half consists of particles streaming directly out of ducts in the torus shell. The latter fraction therefore is highly directional near the walls.

The maximum tolerable counting rate of the soft X-ray proportional counter due to background neutrons and gamma rays is tentatively set to 10^3 counts/s. This value is chosen much smaller than the estimated tolerable background count rate of 5×10^5 s^{-1} (c.f. section 6) because even low intensity spectral lines should be observable. With a sensitive area of the counter of 50 cm^2 (about the size of the soft X-ray beam) and the known detectivity of the counter of a few percent for neutrons and gamma quanta thus the neutron plus gamma ray flux at the counter position must not exceed 10^3 (n + γ)/(cm^2 · s). A reduction of the fluxes by nine orders of magnitude is thus to be achieved by bulk shielding and by designing an efficient labyrinth for the neutrons and gamma rays.

7.2 Proposed Shielding Arrangement

For the double crystal spectrometer (i.e. without spatial scan) a shielding arrangement is proposed (cf. Fig. 13). For the radiation transport estimates it is assumed that the port of the torus used for access is plugged by shielding material with only a hole of 8 cm width by 10 cm height left open. In case that the plugging of the port interferes with other usages of this port, the plug may be substituted by a tightly fitting concrete "collar" around the vacuum tube. This "collar" should be near to the torus and should be large enough to effectively cover the hole port area. This opening is connected by a vacuum pipe through the 2.8 m thick wall to the double crystal set-up in a room adjacent to the torus hall. The size of the duct through the wall will be 9 cm width by 6 cm height.

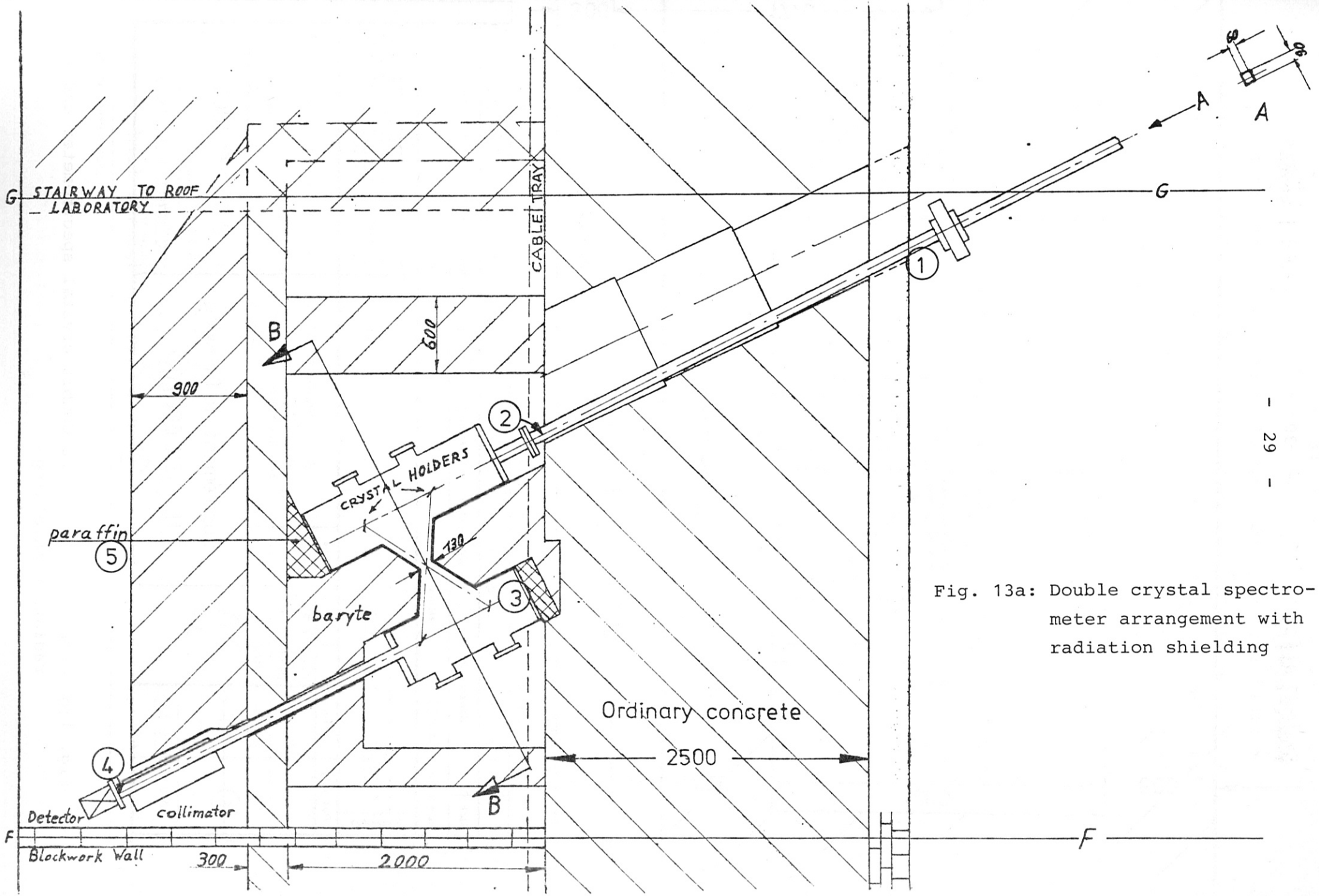

Fig. 13a: Double crystal spectrometer arrangement with radiation shielding

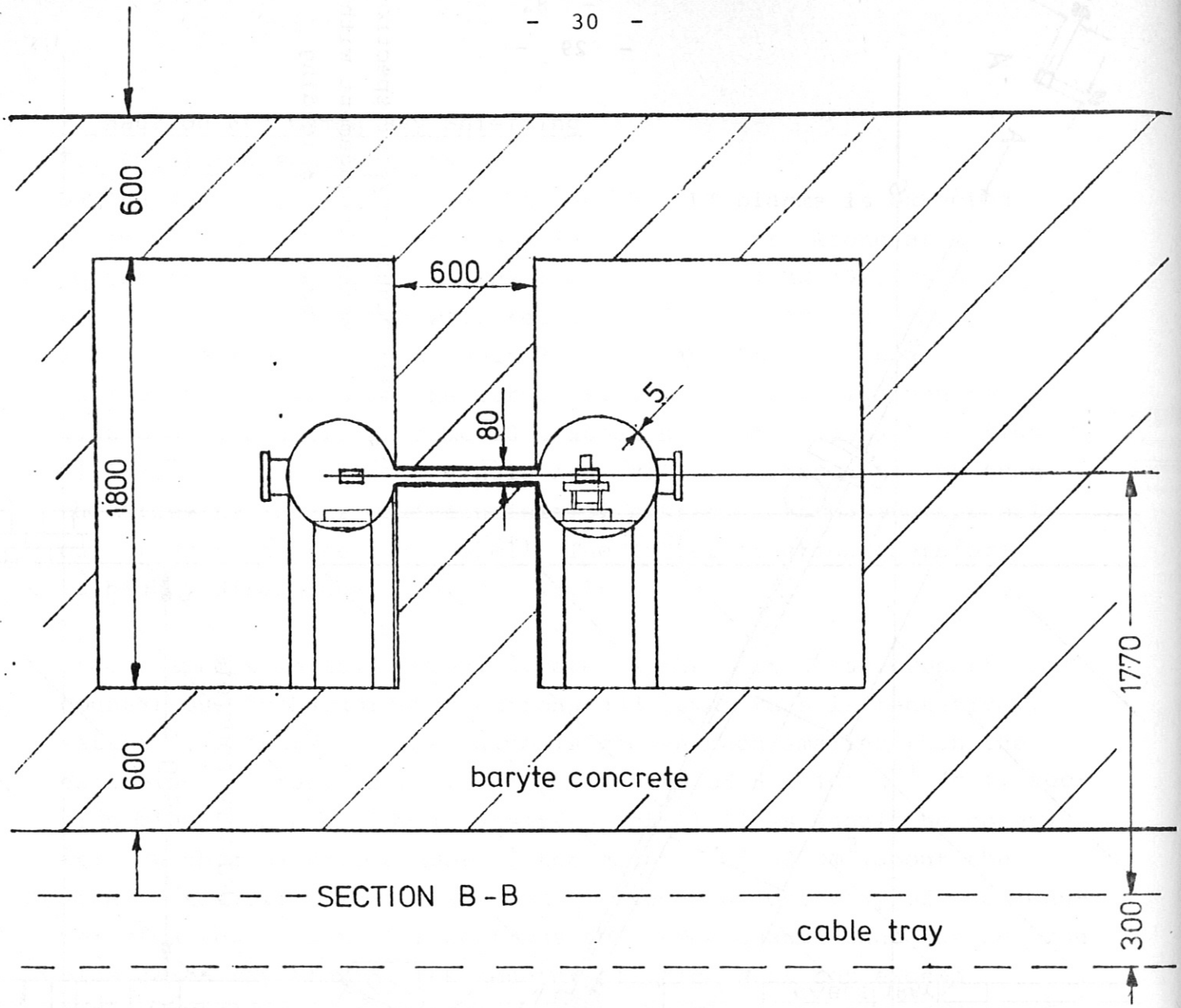

Stck.	Benennung	Zeichnung Nr.	Werkstoff (DIN)	Pos. Nr.	Abmessung, Lager-Nr.	DIN
elektrolytisch poliert ○	relative Permeabilität ≤ 1.					

Änderung

Passung	Abmaß		Datum	Name
		Gez.	1.3.82	J. Fuß
		Bearb.		
		Gepr.		

Max-Planck-Institut für Plasmaphysik
8046 Garching bei München

Bearb. Tel.

Maßstab 1:25

Supplement to Drawing
No. SK 600/004

3 S 1 EC 1004

Ersatz für

Ersetzt durch

Stückl. Nr.

„Satir-Normdruck" 09 6362 80

Fig. 13b: Cross section of the double crystal spectrometer and its radiation shielding

At the rear end of this duct the neutron flux of radiation streaming directly from the port hole through the duct will amount to about 3×10^9 n/(cm^2 · s) with an additional contribution from the isotropic neutron flux in the torus hall of about the same magnitude. For conservativism a flux of 10^{10} n/(cm^2 · s) is therefore assumed at the duct exit (position (2) of Fig. 13a).

The estimates for radiation transport from position (2) to the detector (position (4)) is based on simple geometrical considerations and neutron number albedos as given in table 3. Gamma ray albedos are known to be a few percent at most and thus gamma ray transport can be neglected.

Material	Neutron Number Albedo
Baryte concrete	0.6
Stainless steel, 5 mm thick	0.08
Borated Polyethylene	0.2

Table 3: Neutron number albedos

In a conservative estimation four important radiation transport paths are identified and the shield outlay was adjusted such that each of these paths contributes about the same fraction to the total flux at the detector. These paths are:

(i) Multiple neutron reflections from the vessel of the first crystal through the connection duct into the second crystal vessel to position (3), from there to the detector.

(ii) Same, except that radiation passes through the concrete between the vacuum vessels for the two crystals.

(iii) Neutrons enter the sides of the duct through the wall of the torus hall and move through this wall to position (3), from there to the detector.

(iv) Neutrons pass from the duct through the wall of the torus hall straight to position (5), from there to the detector.

Each of these paths adds a flux contribution of about 1×10^2 $n/(cm^2 \cdot s)$ at the detector position. Together with the flux of gamma quanta created by neutron interactions in the vicinity of the detector a total neutron plus gamma ray flux of only about 1×10^3 $(n + \gamma)/(cm^2 \cdot s)$ can be achieved.

This estimate for the radiation transport in an extraordinary complex geometry as it is represented by this device may not be confused with a proper radiation transport calculation. Its aim was to justify the hope that sufficiently low fluxes can be obtained at the detector position. Further numerical radiation transport calculations are required to reduce some of the conservativism in the estimates and thus to allow possibly significant savings in the cost of the shielding.

7.3 Biological Doses

From the local neutron and gamma ray fluxes biological (equivalent) doses can be derived. Table 4 gives the resulting doses for two years of JET operation with a total of 10^{24} source neutrons being created.

	two year dose
Position (1)	7×10^8 rem
Position (4)	2×10^{-1} rem
Position (5)	2×10^{-1} rem

Table 4: Equivalent doses for two years of JET tritium operation

In case that JET regulations require the doses at position (4) and (5) to be reduced further this can easily be achieved by putting additional concrete around the detector and on the back side of the shielding near position (5) . Each 30 cm of ordinary concrete will result in a dose reduction by one order of magnitude.

8. Double Crystal Device for Continuous Spatial Scan Spectroscopy of JET

A double crystal device in principle can be applied also for continuous spatial scan of the soft-X-ray spectrum, if it is located relatively near to one of the JET flanges. Let us assume, we start from two parallel crystals being set at an arbitrary Bragg angle. If the first crystal is rotated around the light beam axis, i.e. the connexion line of the two crystal centers, it is obvious that the Bragg condition is still conserved. Moreover, the position of the outgoing beam - and hence the detector location - is also conserved. However, the source point can be varied now, e.g. just on a line across the minor cross section of the plasma. Thus continuous spatial scan of the plasma is possible, also for a wide spectral range, if the crystals are guided and rotated as in Fig. 4. The source point does not always describe a straight line across the plasma. This is only the case for a Bragg angle of 45 degrees. For larger or smaller Bragg angles the source point describes a hyperbola with wide opening to the right or left, respectively. If the Bragg angle is denoted by Θ, if z is the coordinate perpendicular to the plane defined by the crystal centers and the outgoing beam (e.g. vertical direction of JET), x the coordinate in this plane (e.g. the azimuthal direction of JET) and a the distance of the first crystal from the source (JET plasma), the hyperbola is described by

$$\frac{\cos^2 2\Theta}{\cos 4\Theta} z^2 + \left(y - \frac{a \cdot \tan 4\Theta}{2}\right)^2 + \frac{a^2}{4} \tan^2 4\Theta = 0.$$

The choice of a system to be proposed strongly depends on the accessibility to the JET plasma.

8.1 Extension of the proposed radiation hardened double crystal spectrometer to a spatially scanning device

Since the estimates of expected count rates for a typical spectral line (cf. section 4) gave relative high values above the background, which allows nearly two orders of magnitude for necessary attenuation, it is suggested to add another double crystal device to the already described spectrometer (cf. Fig.13a), such that the spatial scan device can be plugged in or taken out, if necessary. The arrangement without such additional double crystal device is shown in Fig. 14,

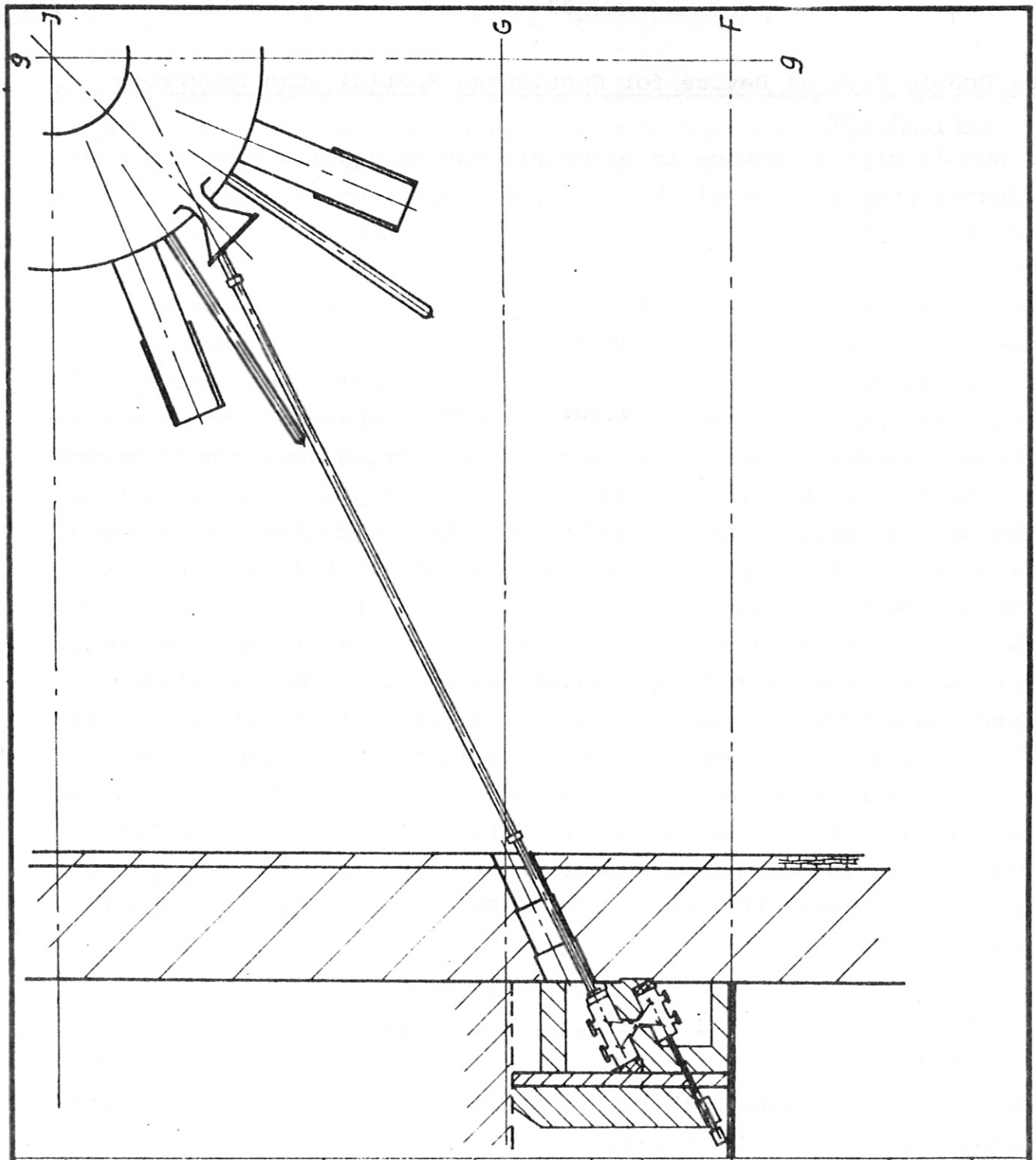

Stck.	Benennung	Zeichnung Nr.	Werkstoff (DIN)	Pos. Nr.	Abmessung, Lager-Nr.	DIN

elektrolytisch poliert ○ | relative Permeabilität ≤ 1,

Änderung

Passung	Abmaß		Datum	Name
		Gez.	25.3.82	
		Bearb.		
		Gepr.		

Max-Planck-Institut für Plasmaphysik
8046 Garching bei München

4 S 1EC 1005

Bearb. Tel.

Maßstab 1:125

Fig. 14 Double crystal spectrometer without spatial scanning

while the extension of this same (radiation hardened) arrangement is completed to a spatial scan broadband crystal spectrometer by an additional crystal pair near the JET flange (octant No. 6 is drawn) as given in Fig. 15. The insert indicates that scanning in vertical direction across most of the minor cross section is possible.

Depending on the choice of the crystals and the wavelength, i.e. the form of the rocking curves, the addition of the two further crystals that facilitate spatial scanning leads to an attention of the Soft-X-ray brightness and hence a reduction of the count rate of up to $P(o)^2/4$, where $P(o)$ is again the crystal peak reflectivity, which for highly reflecting crystals - like Topaz (303) - seems acceptable. For rectangular rocking curves the reduction is given by $P(o)^2$.
Because of these crystals being located near to the JET flange, they will suffer from high neutron and gamma ray fluences. Hence only those crystals can be used that withstand these high fluences. There are crystals like e.g. Quartz, that withstand very high neutron fluences. For Quartz a total neutron fluence of 8×10^{19} n/cm^2 leads to X-ray line shape changes, while smaller neutron fluences do not alter the crystal optical properties of Quartz /11/. This compares with a total neutron fluence of about 4×10^{18} n/cm^2 at the vacuum vessel during two years of JET tritium operation with a production of 10^{24} 14 MeV neutrons. However, especially organic crystals suffer from intense gamma ray radiation /12,13/.

Since the spatial scan addition needs some space of a horizontal JET port , there might be problems of realization of such a device. Therefore the possibility is investigated whether a vertical port can be used for a continuous spatial scan device.

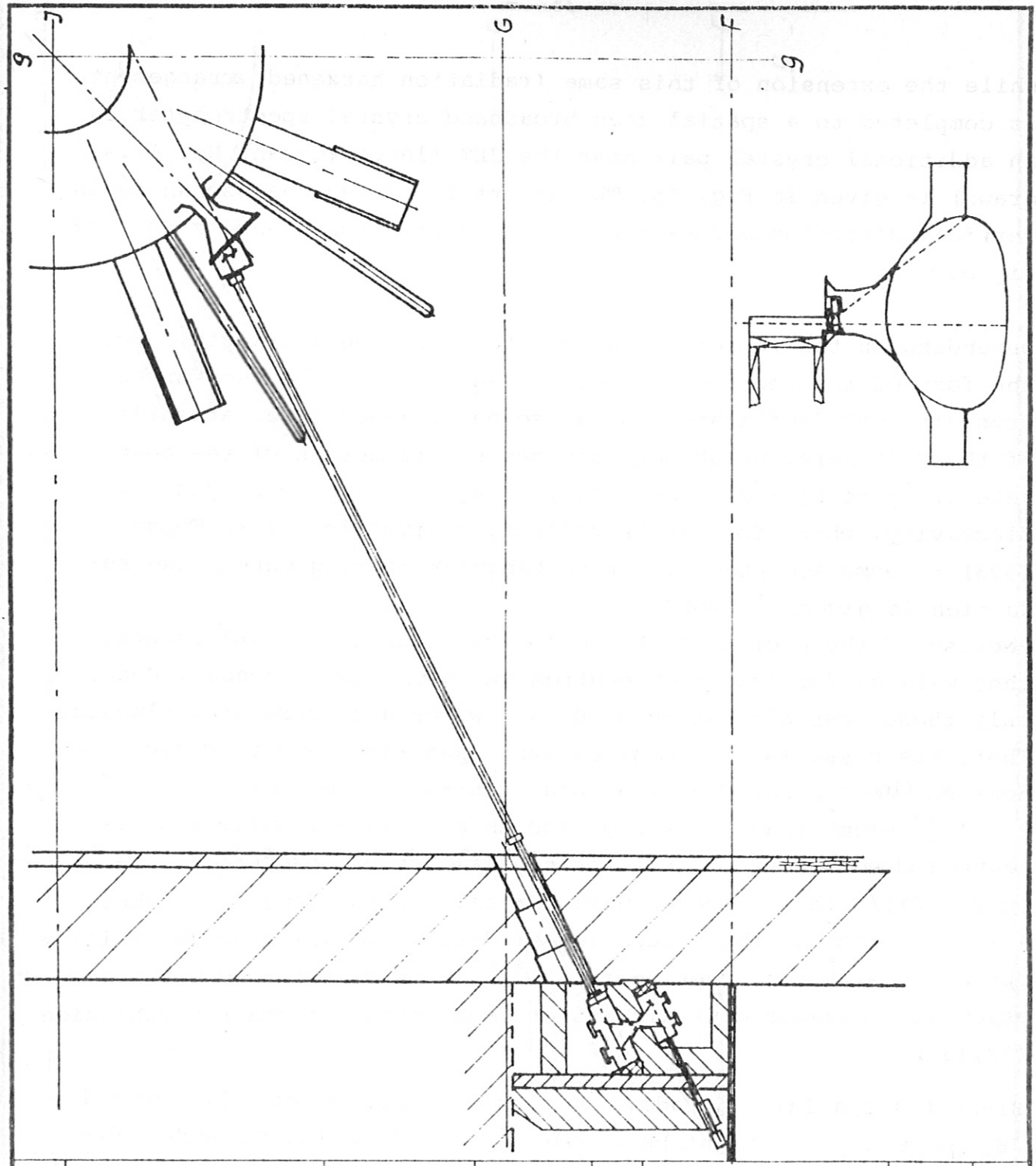

Stck.	Benennung	Zeichnung Nr.	Werkstoff (DIN)	Pos. Nr.	Abmessung, Lager-Nr.	DIN
elektrolytisch poliert ○	relative Permeabilität ≤ 1,					

Änderung

Passung	Abmaß		Datum	Name
		Gez.	25.3.82	
		Bearb		
		Gepr		

Max-Planck-Institut
für Plasmaphysik
8046 Garching bei München

4 S 1EC 1006

Bearb. Tel.

Maßstab 1:125

Fig. 15: Broadband double crystal spectrometer with continuous spatial scanning capability

8.2 Spatial scan double crystal spectrometer for reduced radiation background

Although the addition of another crystal pair for spatial scanning in a "radiation hardened" device is attractive, there might be difficulties with the accessibility to a horizontal diagnostic port. For this reason one might think of a spatial scan Bragg spectrometer with the detector inside the torus hall. Obviously such a device is not applicable in the D-T operation phase of JET because of the high background radiation level. However, for reduced radiation background as for deuterium operation of JET, adequate shielding of the detector appears possible.

Because of the difficulty to make sufficient horizontal port access available such a device would make use of a vertical port, as illustrated in Fig. 16. On top of a valve on this port a vacuum vessel would be installed, which allows a displacement of the Soft X-ray beam by the crystals in azimuthal direction of the JET torus, such that if crystal 1 is rotated around the beam axis, more than the inner radial half axis of the JET plasma can be scanned. The Bragg angle in this version can be scanned from about 12 through 45 degrees. Between the second crystal and the detector a long tube of 5 cm x 5 cm cross section through shielding concrete is foreseen, as sketched in Fig. 16.

Sufficient shielding of the detector in the case of the spatial scan Bragg spectrometer using a vertical port appears very demanding even if its use is restricted to deuterium operation of JET.

Assuming a 2.5 MeV neutron source strength of 5×10^{16} n/s first estimates indicate that the background count rate may be reduced to some 10^4 s^{-1} with 2.5 m of concrete below the detector and about 1.5 m on top of the detector. Through this concrete block, that has to be placed on top of the torus, a vacuum tube (5 cm x 5 cm width) passes from the detector to the second crystal. In order to restrict neutron streaming through this pipe to the detector it is necessary to fill this tube with a neutron collimator (cf. Fig. 16) that consists of planparallel steel plates, 2.5 m long, 5 cm wide and 0.8 mm thick. There is a free spacing of 2.5 mm between adjacent plates. This collimator reduces neutron streaming through the pipe by about a factor of 25 while the optical (soft X-ray) throughput

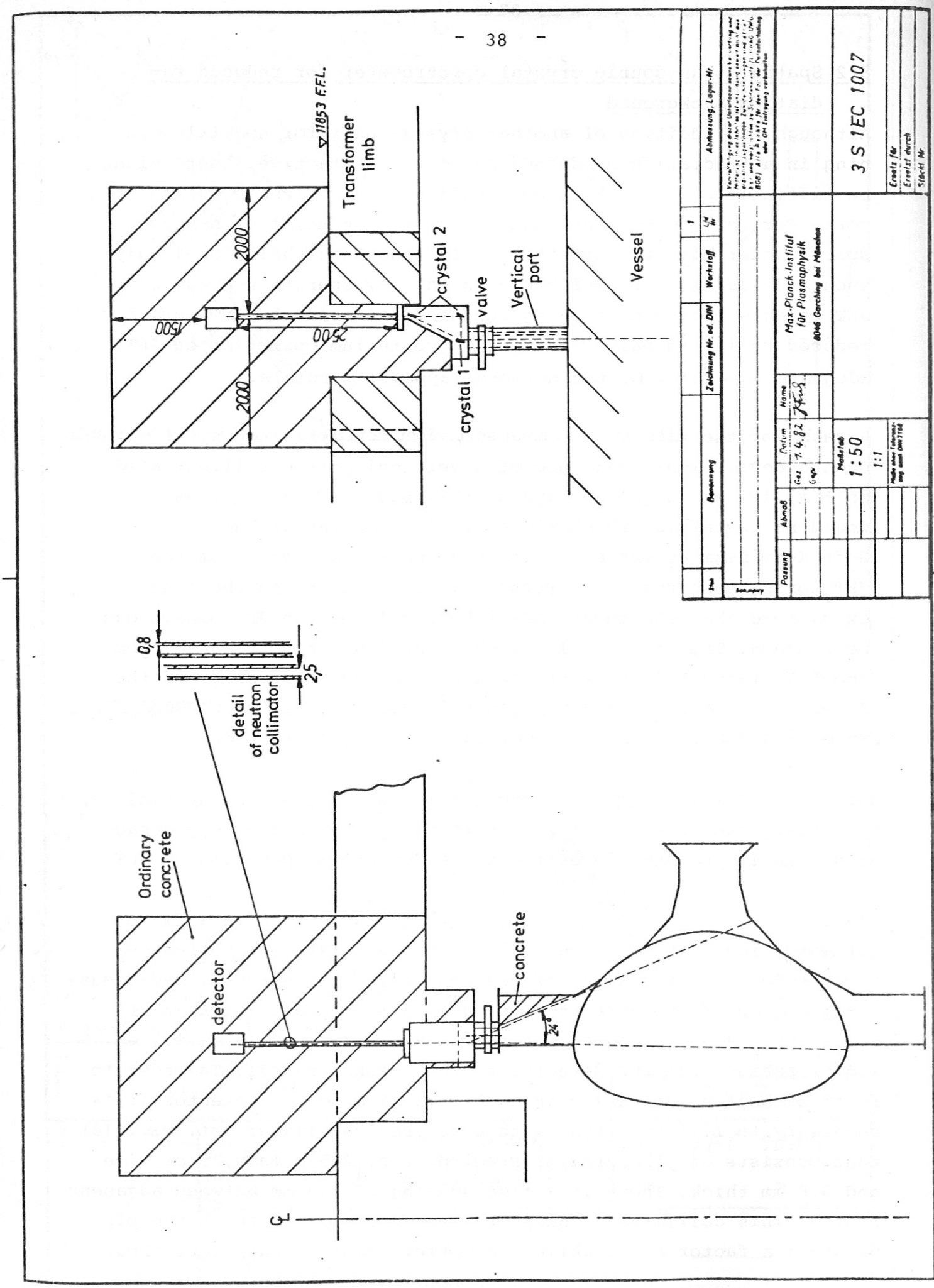

Fig.: 16 Spatial scan Bragg spectrometer arrangement for reduced radiation background

is reduced only insignificantly, since the acceptance angle of 1 mrad of this collimator matches the acceptance angle of the Bragg spectrometer closely.

References:

/1/ A.Burek: Space Science Instrumentation 2, 53 (1976), D.Reidel Publ. Comp. Dordrecht, Holland

/2/ R.Mewe: Astron.Astrophys. 20, 215 (1972)

/3/ C.Breton et al.; EUR-CEA-FC 948 (1978)

/4/ L.Azaroff (ed.): X-Ray Spectroscopy, McGraw-Hill Book Company, New York 1974

/5/ R.Bartimoro, R.Gianella: private communication

/6/ The authors would like to thank Dr.N.Peacock for drawing their attention to this collimator type

/7/ W.Pietsch: private communication

/8/ H.Bradt et al.: Space Science Reviews 8, 471 (1968)

/9/ P.Noll: JET Radiation Levels of Interest for Layout and Maintenance of Electronic Equipment, Codas Handbook, JDN/H (80) 12

/10/ A.Gibson: JET Radiation Levels and their Consequences, JTN/B (79) 139

/11/ E.Lell et al.: Progress in Ceramic Science, Vol. 4 (J.E.Burk ed.) Pergamon Press

/12/ J.Stöhr et al.: Nucl.Instr. and Meth. 152, 43 (1978)

/13/ H.Winick: in Synchrotron Radiation Research (ed. H.Winick and S.Doniach), Plenum Press New York and London, 1980, p.53